INFRARED THERMOGRAPHIC MEASUREMENTS OF HEAT TRANSFER ENHANCEMENT OVER RIBBED SURFACES

L.P.M. Colombo, C. La Briola, A. Niro
Dipartimento di Energetica – Politecnico di Milano, Milan, Italy

Abstract

The paper presents the experimental results on heat transfer characteristics of air forced convection over two ribbed not-thin plates and a flat plate for comparison, obtained by means of infrared thermography. This technique is attractive because it allows a full-field, non-contact, high spatial resolution, measurement of the surface temperature and heat-transfer-coefficient distribution if heat flux distribution is given. In the present case, heat flux is known but at a some depth from the surface convectively cooled while heat diffusion through the plate being not negligible. In this paper, we first present the procedure for processing thermographic images, then its calibration versus convection data over a flat plate, and finally thermal performances of two roughened surfaces with square cross-section ribs perpendicularly arranged to airflow, with two values of the corrugation pitch to rib side ratio, i.e., 33.3 and 13.3. Convection data are for air flows at room temperature with a speed between 2.3 and 11.6 m/s, corresponding to Re_L ranging from 31000 to 155000, and for heat fluxes between 650 and 820 W/m^2.

1 Introduction

Heat transfer in air forced convection over enhanced surfaces is an interesting matter since it is encountered both in devices largely used, such as compact heat exchangers, and in critic applications like the cooling of turbine blades and electronics as well.
Local measurements of heat transfer by convection over complex geometry surfaces are very useful from both a conceptual and a practical standpoint. Indeed, they provide an insight at how fluid dynamics affect heat transfer, and an efficient tool to test thermal performances and to guide geometry optimization of enhanced surfaces. Among the available techniques for heat transfer measurements, infrared thermography is very attractive because it allows a not-intrusive, full-field surveying of the surface temperature with a high spatial resolution. In turn, this measurement brings into determining the local convective heat transfer coefficient, provided that heat flux distribution over the surface is known. However in many cases, heat flux distribution is not exactly known on the surface convectively cooled but at a some depth, while heat diffusion through the material being not negligible. In these cases, both the conductive heat flux and the convective coefficient distribution have to be recovered from the temperature field. This is possible as the conductive heat flux is proportional to the Laplacian of the temperature field. However, in order to get correct evaluations, the noise usually affecting thermographic measurements should be strongly reduced by suitable digital processing of collected images. In the last ten years, many papers, such those by Inagaki and Okamoto (1999), Rainieri and Tartarini (2002), Tanda and Cavallero (2002), were concerned with experimental investigations of heat transfer characteristics by means of both infrared and liquid crystals thermography, and several techniques were proposed for data processing; however, a well established procedure does not exist yet.
This paper presents a work aimed at assessing applicability of thermographic techniques to quantitative heat transfer measurements of not-thin enhanced surfaces. Hence, in the following, first we discuss the procedure set up to evaluate the convective coefficient by thermographic images; then we analyze its calibration versus convection data obtained over a flat not-thin plate; finally, we

present preliminary experimental results on heat transfer characteristics of air forced convection over two ribbed, not-thin plates.

2 Measurement technique basics

Let us consider a flat plate of thickness s which is heated on one side with a fixed heat flux q_o while heat transfer by convection and radiation occurring on the other side; let q_c and q_r be the corresponding heat fluxes. The steady-state energy balance on a parallelepipedal control volume of basis $dxdy$ onto plate surfaces and height s results as follows

$$q_0 dxdy = \left(q_c + q_r\right) dxdy + \int_{z=0}^{z=s} \left(\frac{\partial q_x}{\partial x} dx\right) dydz + \int_{z=0}^{z=s} \left(\frac{\partial q_y}{\partial y} dy\right) dxdz \tag{1}$$

For an homogeneous and isotropic material, if its thermal conductivity k_s is quite independent on temperature, equation (1) becomes

$$q_c = q_0 - q_r + k_s \int_{z=0}^{z=s} \left(\frac{\partial^2 T}{\partial x^2} + \frac{\partial^2 T}{\partial y^2}\right) dz \tag{2}$$

If temperature is also nearly constant along the plate thickness, the Laplacian components result independent on z as well, and equation (2) further reduces to

$$q_c = q_0 - q_r + k_s s \left(\frac{\partial^2 T}{\partial x^2} + \frac{\partial^2 T}{\partial y^2}\right) \tag{3}$$

Because the convective heat flux can be expressed as $q_c=h(T_s-T_a)$ where h is the convective heat transfer coefficient, T_a the air asymptotic temperature and T_s the surface temperature, by substituting this expression in equation (3) and solving for h while keeping in mind $T_s=T(x,y,z=s) \cong T(x,y)$, we get

$$h = \left[q_0 - q_r + k_s s \left(\frac{\partial^2 T}{\partial x^2} + \frac{\partial^2 T}{\partial y^2}\right)\right] \left(T - T_a\right)^{-1} \tag{4}$$

Finally, in considering that q_r too can be evaluated by the surface temperature, in addition to that of surroundings, equation (4) shows the convective coefficient distribution $h(x,y)$ can be reconstructed from the thermal field over the plate, provided that the other quantities are known. Test conditions permitting, it would be convenient to reduce as much as possible heat losses for radiation and conduction in order to make easier evaluation of the convective heat transfer coefficient. However, this is not the present case as the radiative term is small but not negligible, and conduction through the plate plays an important role because of its thickness. Consequently, the temperature Laplacian has to be derived from the thermographic images. However, such a calculation may be complicated because of the noise affecting thermographic images; in fact, the temperature distribution exhibits point-by-point so quick fluctuations that actually make impossible calculating Laplacian unless a filtering procedure is adopted. To this end, both spectral and fitting techniques are suitable and have been applied in this work. A seemingly different approach, that is however just an other way to filter data, consists in approximating h with a known functional form $\tilde{h}\left(x, y; a_1, ..., a_n\right)$, e.g., a polynomial or a power law, where the constant set $\boldsymbol{a}=(a_1,\ldots, a_n)$ is unknown. Rearranging equation (4) in the following and more convenient form

$$k_s s \nabla^2 T - \tilde{h}\left(x, y; a_1, ..., a_n\right)\left(T - T_a\right) - \tilde{q}_r\left(T, T_a\right) + q_0 = 0 \tag{5}$$

it is apparent the unknown is not any longer the convective coefficient h but the temperature distribution $T(x,y)$ which in turn will depend on the constant set $\boldsymbol{a}$. However, these values can be easily found by seeking a convergence between the calculated and measured temperature

distributions, for instance in the least square sense. Once the constant set $\boldsymbol{a}$ is known, of course, the convective coefficient distribution $h(x,y)$ is also fully determined.

3 Experimental setup and measurement procedures

The test section basically consists in a 3 mm thick, 200 mm long, 150 mm wide, aluminum plate. The measurement side is blackened whilst an electric heater, embedded in a silicone rubber, 0.7-mm thick sheet, has been stuck on the other one. To minimize heat losses from the heater backside, this is insulated by a 18-mm thick, cork layer covered in turn by a 1-mm thick, polished aluminum sheet; finally, to ensure mechanical stiffness to the test section, the front and back aluminum plates are tightened together by four teflon screws placed at corners. In the ribbed version 150-mm long, 3 mm ×3 mm cross-section wooden ribs have been arranged transverse to the air flow. Ribs are made of an insulating material so that the only mechanism affecting heat transfer enhancement is the periodic development of the boundary layer tripped by the ribs. The heater is low-voltage DC fed by an HP E3640A power-supply; the maximum rated power is 30 W at 12 V, which corresponds to a heat flux of about 1000 W/m^2. Two K-type thermocouples sheathed in 0.25-mm probes have been placed in two grooves cut in the cork layer, so that they provide a temperature reference on the measurement side, at 1 cm from the trailing edge, and at the centre of the backside plate, respectively.

The test section is positioned in a wind tunnel with the longest side aligned to midline. To reduce flow perturbations over the plate due to the test-section blunt profile, as well as heat losses from its lateral sides, the plate is surrounded with a C-shaped, 3-mm thick frame with a width of 120 mm on the front side, and of 75 mm on the others. The frame is carefully aligned with the plate, and it is linked with the test-section backside by a flat, 20° tilted winglet; finally, the frame leading edge is rounded. The wind tunnel is of closed-circuit type with a contraction ratio of 6:1; airflow has a turbulence intensity lower than 1%, and its speed may be set within 1 and 22 m/s in 0.04-m/s steps since the fan is controlled via an inverter. The test chamber is 80 cm long with a 30 cm × 30 cm squared cross section and Plexiglas walls; onto the wall in front of the test section there is an aperture as large as the plate for optical access, as Plexiglas is opaque to infrared. The optical path from the window to the infrared camera is completely shielded.

The IR-camera is the Raytheon Radiance HS, with a 25-mK sensitivity, InSb Focal Plane Array detector; the acquisition rate is of 140 fps at full resolution, i.e., 256×256 pixels. The IR-camera is calibrated by means of a point source blackbody with an accuracy of 0.1 K. The electrical power supplied to the heater is determined with an accuracy of 0.1 W by measuring the voltage at its terminals as well as across a 2-mΩ calibrated resistor connected in series to the heater. Air speed is measured by a Dantec hot wire anemometer calibrated in a suitable tunnel; the accuracy is near 3%. The air temperature is sensed by a shielded thermocouple placed just upstream the test section, likely in the fluid streaming on its backside. For all the temperature measurements the accuracy is near 0.15 K. Finally, all measurement are performed by means of an Agilent 34970A datalogger with a 6½ digit multimeter.

In spite of the care devoted to make heat losses as small as possible, after each measurement the dissipated power was experimentally determined by the following procedure. First, the frontplate is carefully covered by a 30-mm thick, polystyrene layer; then the heater is powered while air flowing at the same speed as in the test, till the front and backside thermocouples sensed nearly the same temperatures previously reached. We found heat losses vary from 9.3 to 4.1 W, with an error of about 10%, for air speed ranging between 2.3 and 11.6 m/s (as stream velocity increases, the plate mean temperature decreases, and hence thermal dissipations reduce). It is noteworthy these heat loss variations bring about slightly different values of mean heat flux for the various tests as they are all run at the same heating power.

4 Data processing

As already observed, thermal images are affected by noise so that digital filtering is needed to extract affordable data. On this subject, refer for example to Gonzales and Woods (2002). However, great caution must be taken in this operation because filtering, while attenuating noise, distorts the signal as well. The choice of suitable filters depends on the noise nature which, as well known, may be additive or not according to whether it is independent or not on the signal. After a long test series, we defined a filtering procedure described in the following which should overcome the various noise sources affecting this investigation.

Once steady-state conditions are reached, first a 30-images sequence is logged and averaged pixel by pixel. This image number was chosen on the basis of the following considerations. A very long sequences, i.e., 500 images, of the plate at thermal equilibrium with environment was collected, and the average temperature and standard deviation were calculated as functions of the image number N. As a result, the average temperature remains constant with N within a band of 0.02 K, whereas the standard deviation decreases from 0.04 K at N=1 to 0.01 K at N=300, and then it starts to slightly increase (this means ground noise is not purely additive). Finally, at N=30 standard deviation becomes equal to 0.02 K, i.e., the mean-temperature fluctuation band, and hence this is the minimum image number to be collected.

As second step, a median filter with a 9×9 pixels mask is applied (the central pixel value is replaced by the most representative one among the set values, i.e., the median). This filter is very effective in eliminating crazy-pixels and thermal noise; moreover it strongly reduces the risk of creating unrealistic values, that could arise by using averaging techniques; on the contrary, the filtered image results a bit blurred and the finest details can be lost. A further intervention is needed to correct the effect of not uniform heating, which results in bending of constant temperature lines toward the upper and lower edge asymmetrically with respect to the plate horizontal-midline. This asymmetry is not due to free-convection as it jointly rotates with the plate. Hence, temperatures are locally corrected by adding the term

$$\delta T(x,y) \doteq T(x,y) - \overline{T} = \delta T_0 \left(\overline{T} - T_a\right) \Big/ \left(\overline{T} - T_a\right)_0 \tag{6}$$

where T is the measured temperature and $\overline{T}$ its average value over the plate; the index 0 refers to the condition with the plate heated in calm air at such a power rate as its mean temperature approximately equals the value sensed during the test under correction.

After applying median filter, temperature distribution seems to be fairly smooth; however, when the Laplacian is evaluated fluctuations are too large to be acceptable, and hence further filtering of both thermal field and its first derivative is needed. Noise has still a high-frequency content and therefore different low-pass filters were tested starting from the Wiener filter strongly recommended in Rainieri and Pagliarini (2002). However, the best results were obtained by applying a Gaussian filter, i.e., the value of each pixel is weighted with a Gaussian distribution over a square subimage area, that is also referred to as mask, centered on the pixel. The mask dimension can be taken equal to 5 times the standard deviation σ since pixels 2.5σ far from the pivot contribute for near two thousandth. In turn, the standard deviation should be choose on the basis of noise level as the larger σ the higher the smoothing effect. For the present case, the mask size N is determined by a trial-and-error procedure, while keeping as standard deviation the mean of values of σ obtained pixel-to-pixel by averaging temperatures over squared neighborhoods as large as the mask. Best results are found by using a 5x5 mask on the temperature field and a 25x25 mask on its first derivative, and by filtering up to *(N-1)/2* pixels from the edges to avoid windowing effects. As concerns evaluation of the heat transfer coefficient h from equation (5), such is transformed into a system of two first order ordinary differential equations which, once a functional form is adopted for h, are numerically integrated for different values of the constant set $\boldsymbol{a}$ by means of an explicit, one-step, Runge-Kutta method based on the Dormand-Prince schema. Eventually, values of the constant set are refined by least squares fitting of the calculated temperature distributions on experimental data.

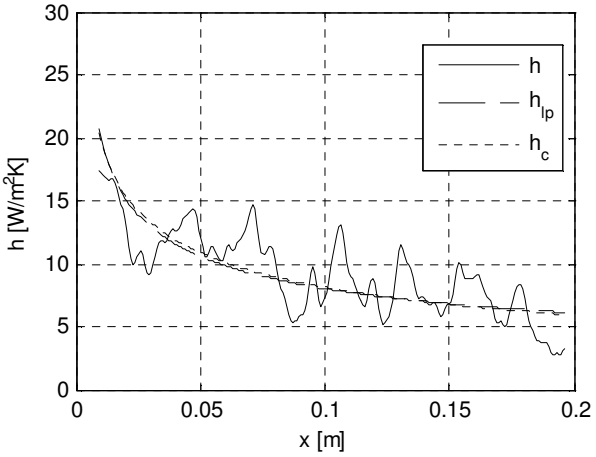

Figure 1. *Local distribution of the heat transfer coefficient for Re=31000 and q=650 Wm^{-2}*

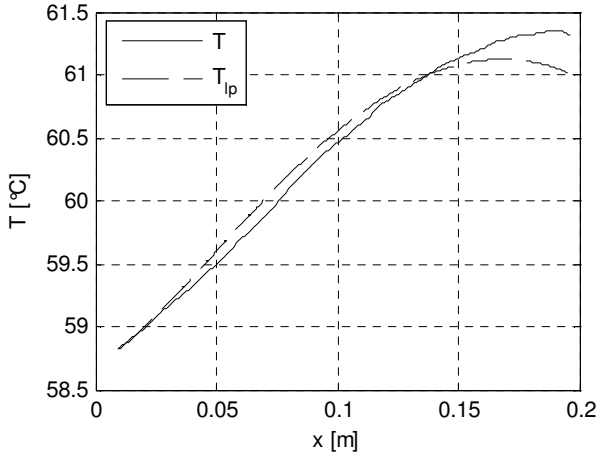

Figure 2. *Measured (T) and calculated temperature (T_{lp}) for Re=31000 and q=650 Wm^{-2}*

5 Experimental results

Presentation of experimental data will start introducing the results for forced convection over a flat plate, used as a benchmark to test the measurement technique. The rib effect will then be considered together with a final comparison and a discussion of the resulting change in heat transfer performances. All the data here presented are for air flows at room temperature with a speed between 2.3 and 11.6 m/s, and for heat fluxes ranging from 650 to 820 W/m^2; as observed, this variability is due to variations in heat losses as the plate is heated on its backside at a constant power rate, and accordingly the higher air velocity the lower the plate temperatures and the heat losses, as well.
Figure 1 shows the distribution of the convective coefficient h over the plate, evaluated by means of Equation 4 and filtering procedure as described above, for a heat flux q=650 W/m^2 and an air speed U=2.33 m/s corresponding to a Reynolds number Re_L=31000. In the figure there also reported two curves respectively obtained with the following correlation

$$h_c\left(x'\right) = Ck\,\mathrm{Pr}^{0.33}\left(\frac{U_\infty}{\nu}\right)^m x'^{m-1}\left[1-\left(\xi/x'\right)^p\right]^{-q} \tag{7}$$

which holds for forced convection over a flat plate with an unheated length ξ, and with this approximated but simpler form

$$h_{lp}\left(x\right) = a\left(x'-\xi\right)^b \simeq h_c\left(x'\right) \tag{8}$$

where x' is the distance from the frame leading edge whereas $x=\left(x'-\xi\right)$ is the local coordinate along the heated portion; exponents p and q amount to 3/4 and 1/3, respectively, in laminar flow regime, whereas in turbulent flow they are 9/10 and 1/9; finally, constant pairs C and m, and a and b are adjusted to least mean squares fit experimental data.
As it can be seen, experimental values of h display significant fluctuations which are entirely due to the Laplacian residual perturbations. However, the mean-absolute-percentage-error, i.e., the mean of the absolute value of percentage error, between experimental data and best-fit values from equation (7) is not so large being equal to 23% with a standard deviation of 2.22 Wm^{-2}K^{-1}; quite similar results are obtained by a comparison with h_{lp}, i.e., ε=24% and σ=2.24 Wm^{-2}K^{-1}.
Figure 2 shows the temperature distribution measured along the plate centerline (more exactly, the mean distribution over the thirty central lines) and for comparison the values calculated with equation (8), which practically coincide with results, not plotted, from equation (7). It is evident there is a good agreement between experimental data and calculations, even though spread tends to increase along the plate; however, the deviation is at most 0.3 K keeping in mind the overall

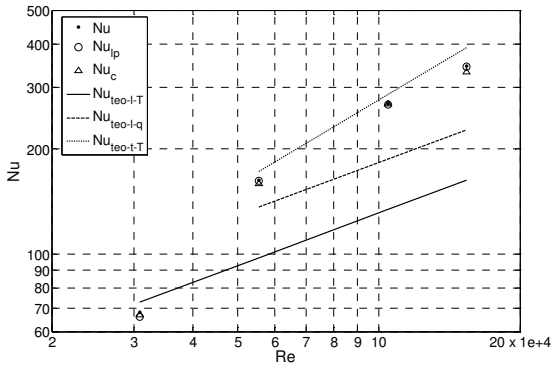

Figure 3. *Average Nusselt number vs Reynolds number for the flat plate*

temperature difference amounts to 2.7 K; furthermore, deviation will vanish by adjusting the constants *a* or *C* of only 1 or 2%.

Analogous trends have been found at air speeds U of 4.2, 7.9 and 11.6 m/s. For increasing values of U, the mean-absolute-percentage-error between experimental and best-fit values increases whereas standard deviation decreases; thus, the values ε=9% and σ=5.10 $Wm^{-2}K^{-1}$ have been found for h_c, whereas for h_{lp} the values ε=12% and σ=7.07 $Wm^{-2}K^{-1}$. As also expected, the temperature difference between the leading and trailing edges decreases as air speed increases, reducing to 1.8 K at U=11.6 m/s.

Finally, the average Nusselt number Nu_L over the plate has been calculated from the experimental heat transfer coefficients; Figure 3 displays these values plotted versus the Reynolds number Re_L. The Nu_L trends in laminar-flow regime for thermal boundary conditions of both uniform temperature and uniform heat flux, as well as in turbulent-flow regime with uniform temperature boundary condition have been calculated from available correlations and represented in the same plot for comparison. The uniform temperature condition has been considered because, as noticed above, the overall temperature along the plate is generally low, i.e., less than 2.7 K, and it decreases with Re_L, whereas heat flux variations are always greater than 10% of its mean value. As a first observation, at Re_L=31000 the experimental value of Nu_L is 9% lower than predicted by theory; such a deviation is fully consistent with experimental errors. Nevertheless, as air speed increases, the difference grows up to 50%, namely, the experimental value of the Nusselt number is always greater than the laminar-flow regime for both boundary conditions of uniform plate temperature and uniform heat flux, while approaching the turbulent-flow values. This behavior is not explained by the difference in thermal boundary conditions between theoretical predictions and actual operation, neither at uniform temperature nor at uniform heat flux. It seems more likely that transition from laminar- to turbulent-flow regime occurs in advance because of perturbations primed by the test section itself in spite of all the cautions; in this respect, it is noteworthy to remark that the opening in front of the

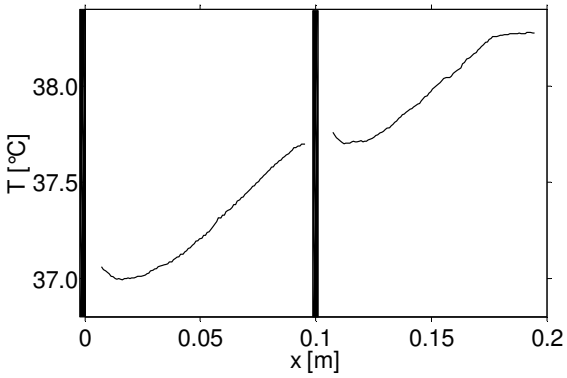

Figure 4. *Temperature distribution along the plate midline for p/e=33.3, q=818 Wm^{-2} and U=7.9 m/s*

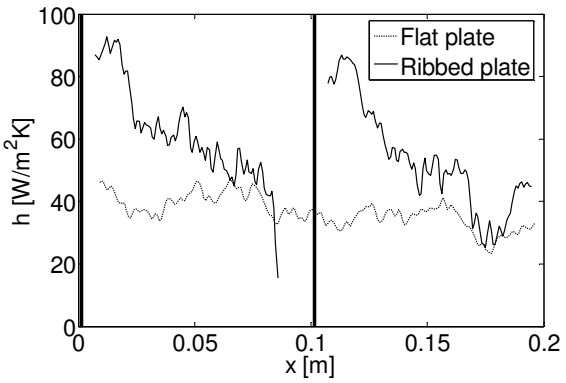

Figure 5. *Heat transfer coefficient distribution along the plate midline for p/e=33.3, q=818 Wm^{-2} and U=7. 9 m/s*

Table 1. *Average heat transfer coefficients for p/e=33.3*

Re_L	h_0 [W/(m^{2}K)]	h [W/(m^{2}K)]	E [%]
31000	8.7	13.9	64.7
55500	20.8	31.9	58.1
105000	34.4	57.3	71.7
155000	44.1	68.8	60.8

Table 2. *Average heat transfer coefficients for p/e=13.3*

Re_L	h_0 [W/(m^{2}K)]	h [W/(m^{2}K)]	E [%]
31000	8.7	18.6	120.4
55500	20.8	34.8	72.5
105000	34.4	52.2	56.4
155000	44.1	59.6	39.3

plate, needed to provide optical access to the IR-camera, could be indeed a disturbance factor.
Now, we proceed to consider the ribbed surfaces. As above reported, ribs have a square cross-section and they are perpendicularly arranged to airflow. Two configurations with two and six ribs, respectively, have been investigated which for simplicity will be referred to by the ratio *p/e* between the corrugation pitch *p* and the rib-cross-section side *e*, namely, *p/e*=33.3 and *p/e*=13.3. For both configurations, the first rib is placed onto the plate leading edge. Experimental tests have been carried out at the same operating conditions as for the flat plate, in order to the results are comparable. Finally, filtering has not been applied to the zones with ribs to avoid introducing thermal field distortions due to their lower temperature; in fact, ribs are made of an insulating material to put in evidence just the influence of velocity-field modifications on heat transfer.
Figure 4 shows as an example the temperature distribution along the plate midline, more precisely the mean distribution over the thirty central lines, for *p/e*=33.3 at q=818 Wm^{-2} and U=7.9 ms^{-1}; the heat flux practically varies within the same range as the flat plate, and the environment temperature is round 23.5°C. As it can be seen, behind the ribs, temperature first slightly decreases and then it grows as far as the successive rib. This behavior is observed without significant differences for all the investigated Reynolds numbers; the mean temperature-increase between the leading and trailing edges is about 1.2 K, i.e., slightly less than the flat plate. The presence of relative minima may be explained in terms of detachment of the fluid vein followed by the new development of the boundary layer; minima occur at a distance from ribs near equal to seven times the rib height, in accordance with what open literature reports. Figure 5 displays the heat-transfer-coefficient distributions along the ribbed plate at the same conditions of Figure 4, along with that for the flat plat; they are representative of all the flow conditions investigated. The behavior obviously reflects the thermal field structure, namely, *h* steeply increases as far as it reaches a marked maximum nearly at the same position where temperature displays the minimum, namely, the fluid-vein reattachment point.

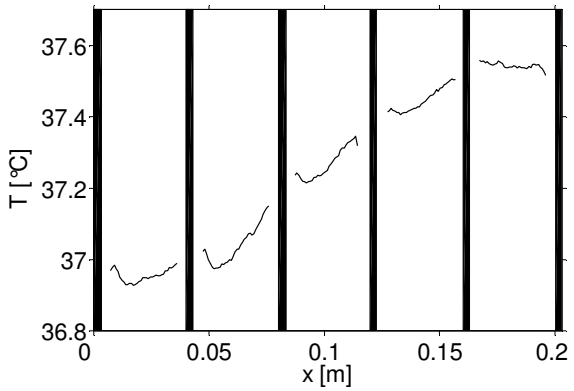

Figure 6. *Temperature distribution along the plate midline for p/e=13.3, q=818 Wm^{-2} and U=7.9 m/s*

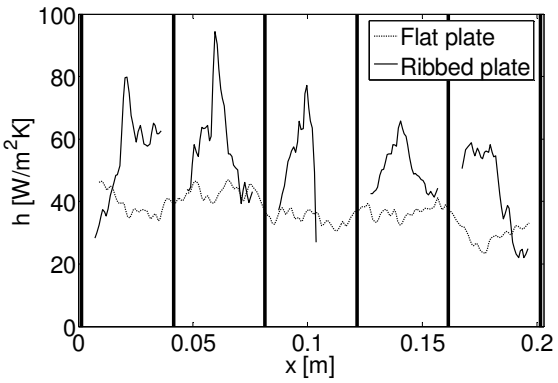

Figure 7. *Heat transfer coefficient distribution along the plate midline for p/e=13.3, q=818 Wm^{-2} and U=7.9 m/s*

Finally, for the investigated Reynolds numbers, Table 1 lists the values of the average heat transfer coefficients $\bar{h}_0$ and $\bar{h}$ for the flat and ribbed plates, respectively, and the enhancement factor $E = \left(\bar{h}L_{eff} / \bar{h}_0 L - 1\right)$ where L_{eff} is the effective length, namely, the plate length without the portion covered by the ribs; L_{eff} corresponds to 3% for *p/e*=33.3 whereas to 9% for the other configuration.
Similarly to Figure 4, Figure 6 shows the midline temperature average-distributions for *p/e*=13.3, q=818 Wm^{-2} and U=7.9 ms^{-1}, whereas Figure 7 presents the corresponding distribution of *h* compared to that for the flat plate. All the qualitative considerations reported for *p/e*=33.3 may be entirely repeated both for the temperature field and heat-transfer-coefficient distribution, whereas peculiar features are the position of h_{max}, falling between the second and third rib for all the Reynolds numbers excepted Re_L=31000, and the maximum locus which seemingly decreases downward the stream. Quantitative comparisons can be drawn from Table 2 which lists the same amounts as the previous table; it is evident that for p/e=13.3 heat transfer enhancement is characterized by a decreasing trend with Re_L.

6 Conclusions

Distributions of heat transfer coefficient in forced convection over flat and ribbed plates have been measured by processing digital thermographic images, and the enhancement factors have been computed. In order to evaluate heat transfer coefficient, an accurate determination of the heat flux distribution from the measured temperature field is needed. On this subject it is worth noting that attention must be paid to data processing as well as to the experimental setup. Actually, suitable but not standardized filtering procedures have to be implemented to correctly evaluate the temperature Laplacian, whereas much care is needed to minimize heat losses from the test section which could significantly affect results. Provided these obstacles are overcome, a fast and not intrusive full field measurement is allowed.

Acknowledgements

The authors are in debt with Mr Damiano Fustinoni for his assistance in the experimental activity. This work is supported by MURST (the Italian Ministry for the University and the Scientific-Technical Research) via PRIN 2005 grants.

References

Gonzalez R.C., Woods R.E., 2002, Digital Image Processing, Upper Saddle River, Prentice Hall.
Inagaki T., Okamoto Y., 1999, Measurement of turbulent heat transfer using infrared thermography near ambient conditions and its quantitative error estimation, Heat Transfer-Asian Research, 28(6).
Kakaç S., Saha R. S., Aung W., 1987, Handbook of single-phase convective heat transfer, New York, Wiley Interscience Publication.
Ranieri S., Pagliarini G., 2002, Data filtering applied to infrared thermographic measurements intended for the estimation of local heat transfer coefficient, Experimental thermal and fluid science, Vol. 26, pp. 109-114.
Tanda G., 2004, Heat transfer in rectangular channels with transverse and V-shaped broken ribs, IJHTM, Vol. 47, pp. 229-243.
Chang S.W., Liou T.-M., Juan W.-J., (2005), Influence of channel-height on heatb transfer augmentation in rectangular channels with two opposite rib-roughened walls, IJHMT, Vol. 48, pp. 2806-2813 .